LETTER

Vertically migrating swimmers generate aggregation–scale eddies in a stratified column

Isabel A. Houghton[1], Jeffrey R. Koseff[1], Stephen G. Monismith[1] & John O. Dabiri[1,2]*

Biologically generated turbulence has been proposed as an important contributor to nutrient transport and ocean mixing[1–3]. However, to produce non-negligible transport and mixing, such turbulence must produce eddies at scales comparable to the length scales of stratification in the ocean. It has previously been argued that biologically generated turbulence is limited to the scale of the individual animals involved[4], which would make turbulence created by highly abundant centimetre-scale zooplankton such as krill irrelevant to ocean mixing. Their small size notwithstanding, zooplankton form dense aggregations tens of metres in vertical extent as they undergo diurnal vertical migration over hundreds of metres[3,5,6]. This behaviour potentially introduces additional length scales—such as the scale of the aggregation—that are of relevance to animal interactions with the surrounding water column. Here we show that the collective vertical migration of centimetre-scale swimmers—as represented by the brine shrimp *Artemia salina*—generates aggregation-scale eddies that mix a stable density stratification, resulting in an effective turbulent diffusivity up to three orders of magnitude larger than the molecular diffusivity of salt. These observed large-scale mixing eddies are the result of flow in the wakes of the individual organisms coalescing to form a large-scale downward jet during upward swimming, even in the presence of a strong density stratification relative to typical values observed in the ocean. The results illustrate the potential for marine zooplankton to considerably alter the physical and biogeochemical structure of the water column, with potentially widespread effects owing to their high abundance in climatically important regions of the ocean[7].

Biologically driven macro-scale flow has been observed in systems ranging from the bio-convective patterns generated by dense bacterial suspensions[8,9] to large-scale induced drift by individually swimming jellyfish[2]. At intermediate length scales, marine zooplankton—which are individually approximately a centimetre in scale—undergo diurnal vertical migration in dense swarms over distances of hundreds of metres[5–7]. Dynamic feedbacks between the zooplankton propulsion and the surrounding flow have the potential to affect the physical and biogeochemical structure of the water column, and they are particularly relevant owing to the presence of diurnal vertical migration in climatically important regions such as the Southern Ocean[7]. Although turbulence created by an individually swimming zooplankton is limited by the length scale of the animal and is therefore primarily dissipated as heat rather than contributing to turbulent mixing[4], the collective migration introduces a new length scale in the form of the vertical height of the swarm, which has previously been observed using acoustic backscatter to span tens of metres[3,5,6].

Although large-scale effects on nutrient distributions, particularly carbon and oxygen, due to the presence of diurnal vertical migration have been reported[7,10,11], direct observations of the fluid dynamics surrounding zooplankton swarms have been limited owing to the difficulty of predicting the precise time and location of a migration event. Building on a previously developed method[12], we conducted laboratory experiments using the representative centimetre-scale swimmers *A. salina* in two stably stratified tank facilities. A 1.2-m-tall tank was used to measure irreversible mixing of the density stratification, and a 2-m-tall tank was used to implement several flow visualization techniques over multiple length scales. In both tanks the strong phototactic response of *A. salina* was leveraged to induce coordinated migrations over the vertical extent of the tank, simulating zooplankton migration through a pycnocline. The 1.2-m tank used an array of focused LEDs with blue filters to form a 10-cm-wide vertical column of light that triggered vertical migration (Fig. 1a). The 2-m tank used a blue laser to form a narrower 5-cm-wide column of light (Fig. 1b). Both light stimuli triggered a similar animal response (for example, in terms of swimming speed and inter-animal spacing), indicating that the migration dynamics were not sensitive to the specific form of visual stimulus.

In experiments measuring irreversible mixing, a stable two-layer stratification was established by using variable-salinity water pumped into the tank in two layers. The average buoyancy frequency across the interface between the two layers (N_{int}) is given by $N_{\mathrm{int}} = \sqrt{-\frac{g}{\rho_0}\frac{\Delta\rho}{\Delta z}}$ in which ρ_0 is the reference density, $\Delta\rho$ is density difference between the top and bottom layer, Δz is the initial interface thickness of 0.2 m used in all cases, and g is gravity. In these experiments, the N_{int} ranged from 0.04 to 0.13 s^{-1}. After stratifying the water column, animals were introduced at a tank-averaged abundance of between 46,000 ± 5,000 animals per m^3 and 138,000 ± 5,000 animals per m^3 in the 1.2-m tank, or 20,000 ± 5,000 animals per m^3 in the 2-m tank, and allowed to acclimatize. Experimental animal abundance was comparable to that observed for a wide variety of ocean zooplankton, which range in abundance[6,13,14] from 10,000 to 70,000 animals per m^3, although local animal densities can be underestimated by orders of magnitude in these types of observations owing to the high spatial heterogeneity in swarms[3,15].

Animals were initially gathered at the bottom of the tank by attracting them with a green LED array introduced to the tank from below. *A. salina* exhibits slight negative buoyancy, similar to most ocean zooplankton, and therefore the animals were minimally active at the bottom of the tank. Initial density profile measurements were then obtained with a vertically traversing density probe located 20 cm laterally from the centre of the LED array (Fig. 1c). Mixing during the filling process smoothed the two-layer stratification interface to produce an error function-like initial density profile (Fig. 2a, black curve).

Animal migration was induced with a blue LED array oriented vertically downward from above the tank, forming a column of light 10 cm in diameter, activated after the deactivation of the green LED array at the bottom of the tank. A strong animal response towards the light occurred, resulting in an upward migration with swimming velocities up to 1 cm s^{-1} (Fig. 1a; see Supplementary Video 1). The distribution of animal reaction times resulted in a vertical spread of animals over the extent of the tank following the activation of the top LED array. After ten minutes, the top blue LED array was deactivated and the bottom green LED array was activated to return the animals to the bottom of the tank. After ten minutes with the animals at the bottom, the bottom

[1]Bob and Norma Street Environmental Fluid Mechanics Laboratory, Civil and Environmental Engineering, Stanford University, Stanford, CA, USA. [2]Mechanical Engineering, Stanford University, Stanford, CA, USA. *e-mail: jodabiri@stanford.edu
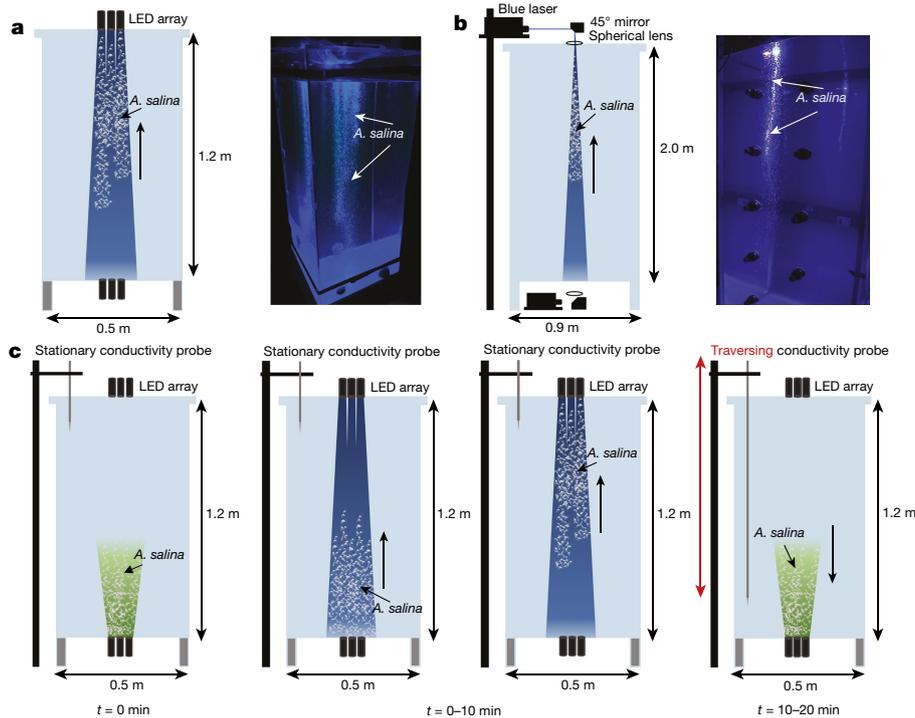
Fig. 1 | Laboratory experiment for controllable vertical migrations. Schematics and images of measurement facilities during experiments are shown. **a**, A $0.5 \times 0.5 \times 1.2$-$m^3$ tank with a two-layer salt stratification was used with an array of 12 focused LEDs with blue filters introduced from the top of the tank, and LEDs with green filters introduced from below for control of the migration. **b**, A $0.9 \times 0.9 \times 2.0$-$m^3$ tank with a linear salt stratification was designed with a blue laser above and green laser below for control of the migration. **c**, Schematic of experimental protocol for measuring irreversible mixing. The 20-min cycle illustrated was repeated six times in total to give a 120-min experiment. A density profile was obtained during each downward migration period. Repeated density profiles were obtained at the end of the experiment to confirm consistency of the density profiles, which indicated that the tank was quiescent and horizontally homogeneous.

green LED array was deactivated and the top blue LED array was once again activated to repeat the up–down migration cycle (Fig. 1c). This cycle was repeated six times in each full experiment lasting 120 min. The duration of the full experiment was selected to match oceanic diurnal vertical migration with a representative swimming speed of $1\,cm\,s^{-1}$ and a representative aggregation with a vertical extent[5] of 50–100 m, leading to a time of approximately 80–170 min for the entire swarm to pass through a fixed depth in the water column that is initially above the aggregation. In the laboratory experiments, the water column was perturbed by the same group of animals multiple times during the 120 min, whereas in an oceanic diurnal vertical migration a given parcel of water is sequentially perturbed by multiple, distinct animals over the 120-min period. Density profiles were obtained each of the six times during the experiment when the animals were at the bottom of the tank, as well as at the end of the experiment. Measured mass changes between initial and final density profiles were limited to ± 6 p.p.m. of total water column mass, attributable to minor probe noise and drift.

The final density profiles after the 120-min experiment exhibited irreversible mixing of the initial density profile. This was indicated by a smoothing of the initial error function density profile; that is, the upper half of the density profile shifted towards higher density and the lower half shifted towards lower density (Fig. 2). Vertically asymmetric mixing occurred with more mixing above the pycnocline than below.

A depth-dependent effective turbulent diffusivity ($\kappa_{eff}(z)$) was used to quantify the effect of swimmer-induced mixing relative to the molecular diffusion of salt (Fig. 3). This empirical effective diffusivity was determined on the basis of a conservative (that is, lower mixing) best-fit numerically integrated density profile to approximate the final experimental profile (see Methods). This conservative estimate yielded effective diffusivities three orders of magnitude larger than the molecular diffusivity of salt.

Flow visualization was used to investigate the processes leading to the observed irreversible mixing. At the scale of the individual swimmer,

Fig. 2 | Density profile temporal evolution. a, Density profiles for $N_{int} = 0.10\,s^{-1}$ taken every 20 min during a 120-min experiment. **b**, Initial and final density profiles for $N_{int} = 0.05\,s^{-1}$ (left) and $N_{int} = 0.10\,s^{-1}$ (right). Shading corresponds to the average scatter of data due to probe measurement uncertainty, with higher relative uncertainty for the lower density difference (left). Higher density stratification results in more asymmetric mixing (right). Normalized density profiles are presented (see Supplementary Methods). **c**, Probability density plots of normalized density corresponding to $N_{int} = 0.05\,s^{-1}$ (left) and $N_{int} = 0.10\,s^{-1}$ (right). Density values shift away from extreme values, indicative of irreversible mixing. Measured mass changes between initial and final density profiles were limited to ± 6 p.p.m. of total water column mass, attributable to minor probe noise and drift.
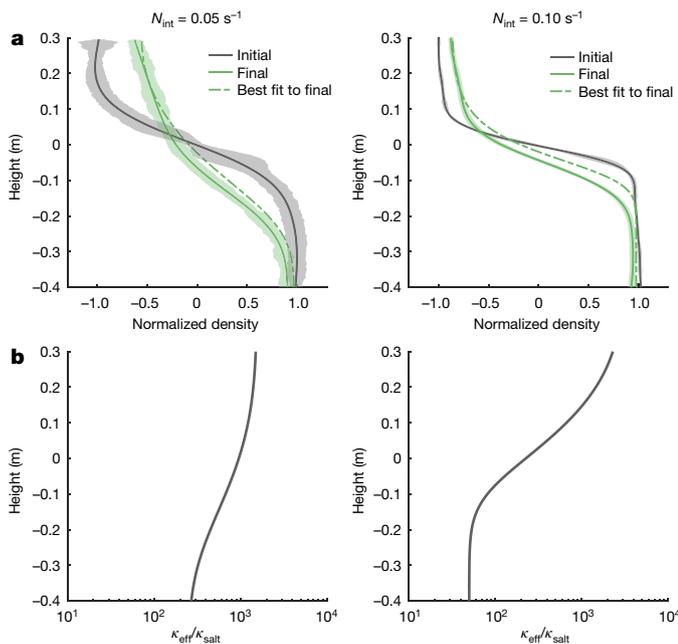
Fig. 3 | Effective diffusivity due to vertical migration. a, Initial (black) and final (solid green) density profiles for $N_{int} = 0.05\,s^{-1}$ (left) and $N_{int} = 0.10\,s^{-1}$ (right). An empirical estimate of effective diffusivity is used for a numerically calculated, best-fit density profile (dashed green; see Supplementary Methods). **b**, Ratio of effective diffusivity to salt molecular diffusivity ($\kappa_{eff}/\kappa_{salt}$) as a function of height for each experiment above. The conservative nature of these estimates is indicated by the smaller shift in the best-fit profile (dashed green curves in **a**) from the initial profiles (black) compared to the final measured profiles (solid green).

A. salina propulsion produces a strong rearward jet (Fig. 4a; see Supplementary Video 2), similar to observed flow fields of zooplankton such as Pacific and Antarctic krill[16]. In the collective migration, a large-scale downward jet developed within the region of upward animal migration owing to the repeated downward fluid displacement by each individual animal propelling itself upward (Fig. 4b–g). Similar to oceanic aggregations[17], downward swimming required less active propulsion owing to the aforementioned negative animal buoyancy, resulting in no aggregation-scale jet during downward migration. This unidirectional formation of a large-scale downward jet during the upward migration resulted in density profiles similar to other asymmetric mixing processes such as horizontal shear at a density interface[18].

Animal proximity in the migration was primarily governed by endogenous animal behaviour, regardless of the light stimulus type and configuration used. The resultant animal spacing was less than the extent of the hydrodynamic signature from an individual animal, similar to observations of Antarctic krill[16]. Owing to this animal proximity, subsequent migrating animals repeatedly interacted with already displaced fluid parcels, propelling fluid further downward and ultimately producing the aggregation-scale rearward jet, characterized by a fluid velocity of 1–2 cm s^{-1}. Outside the organized animal migration, eddying motions at scales an order of magnitude larger than the individual animal were observed (see Supplementary Videos 3–6), similar to flows observed around negatively buoyant plumes[19]. The large-scale eddy motion within the stable density stratification increased the surface area and concentration gradients between the high and low density fluid, enhancing diffusivity and leading to irreversible mixing of the salt concentration at a rate up to three orders of magnitude larger than molecular action alone. For a temperature-stratified water column, irreversible mixing of a thermal stratification is likely to be higher than the mixing measured in the salinity stratification owing to the faster action of thermal diffusivity compared to salt diffusivity[18,20–22].
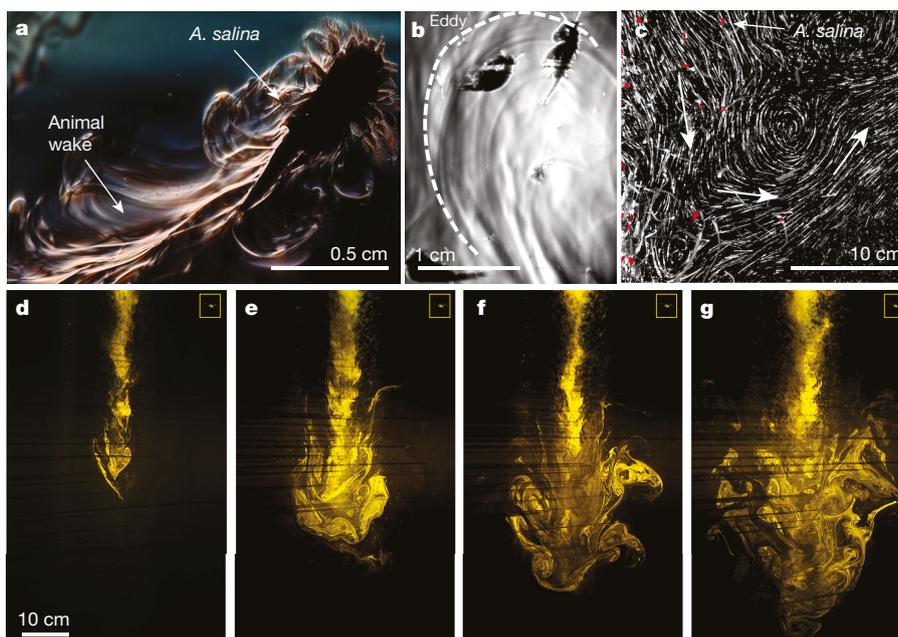
Fig. 4 | Flow visualization from animal to aggregation scales. a, Single animal schlieren image, conducted with the assistance and facilities of R. Strickler, showing fluid motion in the wake of a single animal (see Supplementary Video 2). **b**, Intermediate-scale schlieren imaging with a 5-cm field of view centred 8 cm to the left of the migration, showing the laterally propagating eddies perturbing the stable background density (see Supplementary Video 3). **c**, Pathlines of 10-μm neutrally buoyant particles illustrate the fluid motion to the right of the migration, including the downward jet proximate to the aggregation and eddy motion on the periphery. Individual swimmers are overlaid in red. White arrows show flow direction (see Supplementary Video 5). **d–g**, Planar cross-section of laser-induced fluorescence of a tracer dye propelled downward through the extent of the migration at $t = 54\,s$ (**d**), 122 s (**e**), 185 s (**f**) and 292 s (**g**). Surface fluid is propelled vertically downward more than 50 cm through a stable stratification, with large-scale flow structures entraining fluid proximate to the downward jet. Animals in the laser sheet cast horizontal shadows through the illuminated dye. Individual animal size is highlighted in the inset in the upper right hand corner. All imaging methods are described in detail in the Supplementary Methods.

Laboratory experiments in both the 1.2-m-tall and 2-m-tall tank consistently showed that the downward jet propagated throughout the full vertical extent of the aggregation, that is, wherever animals were present to repeatedly propel fluid downward, even within a strong background stratification relative to typical values observed in the ocean. For an oceanic aggregation of zooplankton, flow developing over this extent would correspond to a vertical span of tens of metres. Because diurnal vertical migrations often extend from the surface to depths of 600 m or deeper[7], the diurnal passage of zooplankton could potentially induce large-scale vertical motion and mixing in regions of high nutrient, microbial and density variability. Such transport and mixing would have important feedbacks for local growth and productivity, thereby affecting regional marine biogeochemistry[23–25].

Moreover, the irreversible mixing observed due to the passage of an aggregation of swimmers has potential implications for physical feedbacks with the density stratification, for example, by changing local dynamics and driving regional flow. The global presence of diurnal vertical migration[7], the substantial horizontal and vertical span of aggregations[6], and the frequent occurrence of migrations presents a mechanism for non-negligible mixing across stabilizing gradients, with numerous potential effects on the physical and biogeochemical structure of the ocean. It remains to observe these mechanisms in situ; however, recent reanalyses of echosounder and acoustic Doppler current profiler measurements suggest that the signature of biogenic ocean mixing is ripe for discovery[17].

Online content

1. Dewar, W. K. et al. Does the marine biosphere mix the ocean? *J. Mar. Res.* **64**, 541–561 (2006).
2. Katija, K. & Dabiri, J. O. A viscosity-enhanced mechanism for biogenic ocean mixing. *Nature* **460**, 624–626 (2009).
3. Huntley, M. E. & Zhou, M. Influence of animals on turbulence in the sea. *Mar. Ecol. Prog. Ser.* **273**, 65–79 (2004).
4. Visser, A. W. Biomixing of the oceans? *Science* **316**, 838–839 (2007).
5. Sato, M., Dower, J. F., Kunze, E. & Dewey, R. Second-order seasonal variability in diel vertical migration timing of euphausiids in a coastal inlet. *Mar. Ecol. Prog. Ser.* **480**, 39–56 (2013).
6. Hamner, W. M., Hamner, P. P., Strand, S. W. & Gilmer, R. W. Behavior of antarctic krill, *Euphausia superba*: chemoreception, feeding, schooling, and molting. *Science* **220**, 433–435 (1983).
7. Bianchi, D., Galbraith, E. D., Carozza, D. A., Mislan, K. A. S. & Stock, C. A. Intensification of open-ocean oxygen depletion by vertically migrating animals. *Nat. Geosci.* **6**, 545–548 (2013).
8. Pedley, T. J. & Kessler, J. O. Hydrodynamic phenomena in suspensions of swimming microorganisms. *Annu. Rev. Fluid Mech.* **24**, 313–358 (1992).
9. Koch, D. L. & Subramanian, G. Collective hydrodynamics of swimming microorganisms: living fluids. *Annu. Rev. Fluid Mech.* **43**, 637–659 (2011).
10. Zhang, X. & Dam, H. G. Downward export of carbon by diel migrant mesozooplankton in the central equatorial Pacific. *Deep Sea Res. Part II Top. Stud. Oceanogr.* **44**, 2191–2202 (1997).
11. Longhurst, A. R. & Glen Harrison, W. Vertical nitrogen flux from the oceanic photic zone by diel migrant zooplankton and nekton. *Deep Sea Res. A* **35**, 881–889 (1988).
12. Wilhelmus, M. M. & Dabiri, J. O. Observations of large-scale fluid transport by laser-guided plankton aggregations. *Phys. Fluids* **26**, 101302 (2014).
13. Hanamura, Y., Endo, Y. & Taniguchi, A. Underwater observations of the surface swarm of a euphausiid, *Euphasia pacifica*, in Sendai Bay, northeasterern Japan. *Mer (Paris)* **22**, 63–68 (1984).
14. Kunze, E., Dower, J. F., Beveridge, I., Dewey, R. & Bartlett, K. P. Observations of biologically generated turbulence in a coastal inlet. *Science* **313**, 1768–1770 (2006).
15. Omori, M. & Hamner, W. M. Patchy distribution of zooplankton: behavior, population assessment and sampling problems. *Mar. Biol.* **72**, 193–200 (1982).
16. Catton, K. B., Webster, D. R., Kawaguchi, S. & Yen, J. The hydrodynamic disturbances of two species of krill: implications for aggregation structure. *J. Exp. Biol.* **214**, 1845–1856 (2011).
17. Tarling, G. A. & Thorpe, S. E. Oceanic swarms of antarctic krill perform satiation sinking. *Proc. R. Soc. B* **284**, 20172015 (2017).
18. Jackson, P. R. & Rehmann, C. R. Experiments on differential scalar mixing in turbulence in a sheared, stratified flow. *J. Phys. Oceanogr.* **44**, 2661–2680 (2014).
19. Turner, J. S. Jets and plumes with negative or reversing buoyancy. *J. Fluid Mech.* **26**, 779–792 (2006).
20. Shih, L. H., Koseff, J. R., Ivey, G. N. & Ferziger, J. H. Parameterization of turbulent fluxes and scales using homogeneous sheared stably stratified turbulence simulations. *J. Fluid Mech.* **525**, 193–214 (2005).
21. Nash, J. D. & Moum, J. N. Microstructure estimates of turbulent salinity flux and the dissipation spectrum of salinity. *J. Phys. Oceanogr.* **32**, 2312–2333 (2002).
22. Aref, H. & Jones, S. W. Enhanced separation of diffusing particles by chaotic advection. *Phys. Fluids A* **1**, 470–474 (1989).
23. Moore, C. M. et al. Processes and patterns of oceanic nutrient limitation. *Nat. Geosci.* **6**, 701–710 (2013).
24. DeLong, E. F. Microbial community genomics in the ocean. *Nat. Rev. Microbiol.* **3**, 459–469 (2005).
25. Fuhrman, J. A., Cram, J. A. & Needham, D. M. Marine microbial community dynamics and their ecological interpretation. *Nat. Rev. Microbiol.* **13**, 133–146 (2015).

METHODS

No statistical methods were used to predetermine sample size. The experiments were not randomized and the investigators were not blinded to allocation during experiments and outcome assessment.

Laboratory migration systems. The following systems were used to create the laboratory migrations.

LED array animal guidance. Animal guidance in the 1.2-m-tall tank consisted of two arrays of LEDs with focusing optics with approximately 250-mm focal length (Outlite a100) and blue and green filters arranged to illuminate a ten-centimetre-square area. One LED array was used at a time to induce unidirectional swimming towards the top (blue LEDs) or bottom (green LEDs) of the tank.

Laser animal guidance. Animal guidance in the 2-m-tall tank consisted of two lasers. A 1-W, 447-nm (blue) laser was mounted horizontally above the tank and aligned with a −50-mm focal length spherical lens (Newport Optics) and a 45° mirror to redirect the beam vertically downward in the centre of the water column. A 1-W, 532-nm (green) laser was mounted horizontally beneath the tank with identical optics to redirect the beam vertically upward. The blue and green laser beams were centred and aligned throughout the height of tank. One laser was used at a time to induce unidirectional swimming towards the activated laser, that is, towards the top blue laser or bottom green laser.

Animal protocol. Adult-sized *A. salina*, commonly known as brine shrimp, were obtained before each experiment (Mariculture Tech) and allowed to acclimatize in aerated beakers for at least 3 h at a salinity similar to that used in the experiment (26‰). The animals were then introduced at the top of the tank and allowed to further acclimatize before commencing an experiment. In the 1.2-m tank, animals were introduced at a tank-averaged abundance of 46,000 ± 5,000 animals per m³ to 138,000 ± 5,000 animals per m³. Irreversible mixing measurements were insensitive to the range of animals introduced to the tank in these experiments. In the 2-m tank, animals were introduced at a tank-averaged abundance of 20,000 ± 5,000 animals per m³.

Tank stratification and density measurements. All experiments used salt to produce the density stratification and held the temperature at a constant 21 °C, matching ambient laboratory conditions. For measurements of irreversible mixing, the 1.2-m-tall tank was stratified with variable-salinity water to form two layers of distinct density, similar to setups for a variety of laboratory mixing experiments in the literature[26,27]. The lighter layer (26.0‰) was first pumped into the tank followed by the denser layer (26.3 ± 0.2‰) pumped in from below. For flow visualization, the 2-m-tall tank was linearly stratified using a double bucket technique[28] between 25.6‰ of salt at the surface and 26.2‰ of salt at a depth of 2 m, yielding a buoyancy frequency of $N = 0.05\,\mathrm{s}^{-1}$. Animal swimming behaviour and the large-scale jet formation were unaffected by the stratification type used (that is, two-layer or linear).

A conductivity–temperature profiler (125MicroScale Conductivity and Temperature Instrument (MSCTI), Precision Measurement Engineering) was used to measure the local density with an accuracy of $\pm 0.005\,\mathrm{kg\,m}^{-3}$. To minimize probe drift due to exposure to air, the 6-cm span of the probe tip was continuously immersed in the tank, restricting measurements to 6 cm below the surface. Density profiles were linearly extrapolated 6 cm to the surface in post-processing for evaluation of mass conservation. The raw data points were used to calculate the water column mass while a spline fit with uncertainty bounds was used for the displayed density profiles. To obtain the normalized density profiles presented, the location of peak stratification of the initial density profile was found and the density and height values were shifted such that this location passed through the origin. Density was then rescaled to span [−1,1] following the expression,

$$\rho_{\mathrm{normalized}} = \frac{\rho_{\mathrm{raw}} - \rho_{\mathrm{peak}}}{(\rho_{\mathrm{max}} - \rho_{\mathrm{min}})/2} \tag{1}$$

in which ρ_{raw} is the raw density data, ρ_{peak} is the density at the peak stratification, ρ_{max} is the highest density (density of the bottom layer) and ρ_{min} is the lowest density (density of the top layer). All subsequent profiles in the same experiment were shifted and rescaled with values (ρ_{peak}, ρ_{max} and ρ_{min}) from the initial profile.

Density profiles were obtained at the end of each ten minute downward migration cycle. For quantitative analysis of mass conservation and irreversible mixing, repeated final profiles were obtained every ten minutes after the 120-min experiment until it was confirmed that density profiles were constant in time, signalling that the tank was fully settled and horizontally homogeneous. The 120-min experiment was conducted six times. The density differences between the top and bottom layers in each experiment were 0.03 kg m⁻³ ($N_{\mathrm{int}} = 0.04\,\mathrm{s}^{-1}$), 0.05 kg m⁻³ ($N_{\mathrm{int}} = 0.05\,\mathrm{s}^{-1}$), 0.16 kg m⁻³ ($N_{\mathrm{int}} = 0.09\,\mathrm{s}^{-1}$), 0.21 kg m⁻³ ($N_{\mathrm{int}} = 0.10\,\mathrm{s}^{-1}$), 0.22 kg m⁻³ ($N_{\mathrm{int}} = 0.10\,\mathrm{s}^{-1}$) and 0.36 kg m⁻³ ($N_{\mathrm{int}} = 0.13\,\mathrm{s}^{-1}$). For the experiment with a density difference of 0.16 kg m⁻³ ($N_{\mathrm{int}} = 0.09\,\mathrm{s}^{-1}$), two 30-min upward migrations were induced instead of six 10-min upward migrations, to study the effect of migration duration. The final density profile was consistent for the two experiments with the same cumulative upward migration time. For experiments with similar stratification strength ($N_{\mathrm{int}} = 0.09$, $N_{\mathrm{int}} = 0.10$ and $N_{\mathrm{int}} = 0.10$) the normalized density profiles collapsed onto the same shape. When overlaying the normalized density profiles, the standard deviation of the normalized density measurements for the three different experiments was approximately 6.8 per cent for the initial profiles and 6.9 per cent for the final profiles, indicating the profiles evolved similarly in each experiment.

Calculation of effective diffusivity. Depth-independent effective diffusivity, calculated from an error function fit to the final density profiles, was of order $10^{-2}\,\mathrm{cm}^2\,\mathrm{s}^{-1}$, three orders of magnitude larger than the molecular diffusivity of salt. However, a constant effective diffusivity with an initial error-function density profile yields symmetric error-function final profiles. Thus, these estimates produced poor fits to the spatial variability of the experimental data. To improve the estimate, a depth-dependent effective diffusivity was used. A numerical integrator (MATLAB, Mathworks) solved the diffusion equation,

$$\frac{\partial C}{\partial t} = \frac{\partial}{\partial z}\left(\kappa_{\mathrm{eff}}(z)\frac{\partial C}{\partial z}\right)$$

using a forward-in-time, centred-in-space explicit numerical scheme to obtain final density profiles from the initial experimental profiles and a prescribed effective diffusivity, $\kappa_{\mathrm{eff}}(z)$. A simulated annealing algorithm (MATLAB, Mathworks) was used to minimize the norm of the difference between the experimental final profile and the numerically calculated final profile with a depth-dependent effective diffusivity. This method informed the general shape of effective diffusivity with height, yielding approximately an error-function-shape effective diffusivity profile with the highest values above the pycnocline. We then empirically optimized the general shape obtained from the simulated annealing algorithm with a parameter sweep of constants defining the shift, spread and amplitude of an error function. This optimization was done to obtain a conservative estimate of effective diffusivity, that is, chosen to underestimate effective diffusion, particularly in regions where the full asymmetry of the profile was difficult to capture numerically. Peak values of the depth-dependent effective diffusivity were the same order of magnitude as the calculated depth-independent effective diffusivity.

Flow visualization. The following techniques were used for flow visualization.

Schlieren imaging. Density gradients in the flow were visualized with a schlieren imaging setup with a field of view of 5 cm in the 2-m-tall tank. A 75-W Xenon arc lamp was used to illuminate the field. The light passed through a condenser lens and horizontal slit and then was collimated via a 250-mm focal length plano-convex doublet lens (Newport Optics). The resultant 5-cm diameter parallel light beam travelled through the width of the tank at a height 1 m above the bottom of the tank and was distorted by the varying indices of refraction of the perturbed density field in the path of the light. The beam then passed through a 400-mm focal length plano-convex doublet lens that converged the beam to a focal point. A precision aligner was used to position a vertical razor blade at the focal point of the beam. For the varying density flow, the deflected rays do not coincide with the focal point and were either blocked by the razor blade or passed through without any reduction in intensity, depending on the density gradients encountered[29]. The total light distortion over the path length yielded an image with regions of higher and lower illumination corresponding to regions of the highest positive and negative fluid density gradients, respectively, in the direction normal to the razor blade edge (that is, horizontally).

Single animal schlieren (Fig. 4a and Supplementary Video 2) was conducted with the assistance and facilities of R. Strickler (University of Wisconsin, Milwaukee) with a free swimming animal in a 10 × 5 × 15-cm tank linearly stratified from 0‰ at the surface to 35‰ at a depth of 15 cm. The schlieren setup was similar to that described above except with 250-mm and 150-mm focal length plano-convex doublet lenses creating a 1.5-cm field of view. The considerably stronger density stratification and smaller field of view produced a much stronger and clearer schlieren signal than in the larger-scale experiments with no observable effect on swimming behaviour.

Tracer particle overlay. The 2-m-tall tank was seeded with 10-μm glass beads and illuminated with a vertical red laser sheet formed with a cylindrical lens with a focal length $f = -9.7\,\mathrm{mm}$ (Newport Optics) resulting in a vertical sheet height of 40 cm at the location of the migration. *Artemia* response to red wavelengths is minimal, so animal behaviour was unaffected by the additional laser. A camera (Nikon D750, 24 megapixel) with a focal length $f = 14$-mm lens (Nikon AF Nikkor) was used to record video focused to the right of the migration when viewed on camera. The wide field of view of the lens resulted in image distortion that was removed during post-processing. Sets of 250 consecutive frames, corresponding to 4.2 s of video, were overlaid by storing the maximum illumination of each pixel in the stack resulting in streaks representing the pathlines of particles in the flow. Swimming animals in the frames resulted in wider grey streaks much larger than the actual

individual size. Animals from the final frame were overlaid and highlighted in red to illustrate relative size.

Planar-laser-induced fluorescence. Planar-laser-induced fluorescence was used to obtain an aggregation-scale view of the resultant hydrodynamics in the 1.2-m tank. A 532-nm (green) laser with an $f = -25$-mm plano-concave cylindrical lens (Newport Optics) created a laser sheet illuminating fluorescent dye (Rhodamine 6 G, Sigma-Aldrich) in the tank. Animals had a stronger phototactic response to the blue LED array, so introduction of the green sheet laser during an upward migration did not affect animal behaviour. Qualitative visualization of the transport through an animal aggregation was conducted with 3 ml of 500 p.p.m. Rhodamine 6 G dye slowly introduced at the water surface with a horizontally oriented pipette such that the dye had no initial vertical momentum. In a quiescent tank (or with the aggregation at the bottom of the tank), the buoyant dye spread into a very thin layer at the top of the tank and remained there with very minor diffusion ($D_{\text{Rh6G}} \approx 10^{-10}\,\text{m}^2\,\text{s}^{-1}$). As an upward migration developed, the animals propelled fluid rearward, eventually transporting the dye from the surface downward through the entire extent of the migration. An orange filter placed over the camera (Nikon D750, 24 megapixel) isolated the fluorescent signal from the dye. Flow patterns were recorded in real-time at 60 frames per second as experiments were carried out.

Reporting summary. Further information on experimental design is available in the Nature Research Reporting Summary linked to this paper.

Data availability. Density profile data are available at https://github.com/ihoughton/Houghton2018_data. All other data are available from the corresponding author upon reasonable request.

26. Linden, P. F. Mixing across a density interface produced by grid turbulence. *J. Fluid Mech.* **100**, 691–703 (2006).
27. Whitehead, J. A. & Stevenson, I. Turbulent mixing of two-layer stratified fluid. *Phys. Fluids* **19**, 125104 (2007).
28. Economidou, M. & Hunt, G. R. Density stratified environments: the double-tank method. *Exp. Fluids* **46**, 453–466 (2009).
29. Settles, G. S. *Schlieren and Shadowgraph Techniques* (Springer, Berlin, 2001).

naturе research

Corresponding author(s): Isabel A. Houghton, Jeffrey R. Koseff, Stephen G. Monismith, John O. Dabiri

☐ Initial submission ☒ Revised version ☐ Final submission

Life Sciences Reporting Summary

Nature Research wishes to improve the reproducibility of the work that we publish. This form is intended for publication with all accepted life science papers and provides structure for consistency and transparency in reporting. Every life science submission will use this form; some list items might not apply to an individual manuscript, but all fields must be completed for clarity.

For further information on the points included in this form, see Reporting Life Sciences Research. For further information on Nature Research policies, including our data availability policy, see Authors & Referees and the Editorial Policy Checklist.

▶ Experimental design

1. Sample size

   Describe how sample size was determined.

   > Animal migration experiments were repeated six times under a variety of parameters. Each experiment produced the same result within the parameter range. This convergence of results led us to conclude the tests.

2. Data exclusions

   Describe any data exclusions.

   > Two representative cases are presented in the manuscript in their entirety.

3. Replication

   Describe whether the experimental findings were reliably reproduced.

   > One attempt at replication failed, attributable to a reduced phototactic response of the animals.

4. Randomization

   Describe how samples/organisms/participants were allocated into experimental groups.

   > No experimental groups were used. Each repeated experiment was conducted in subsequent weeks with a different batch of animals.

5. Blinding

   Describe whether the investigators were blinded to group allocation during data collection and/or analysis.

   > Blinding was not relevant because randomized groups were not used.

   Note: all studies involving animals and/or human research participants must disclose whether blinding and randomization were used.

6. Statistical parameters

   For all figures and tables that use statistical methods, confirm that the following items are present in relevant figure legends (or in the Methods section if additional space is needed).

n/a	Confirmed	
☒	☐	The exact sample size (n) for each experimental group/condition, given as a discrete number and unit of measurement (animals, litters, cultures, etc.)
☐	☒	A description of how samples were collected, noting whether measurements were taken from distinct samples or whether the same sample was measured repeatedly
☐	☒	A statement indicating how many times each experiment was replicated
☒	☐	The statistical test(s) used and whether they are one- or two-sided (note: only common tests should be described solely by name; more complex techniques should be described in the Methods section)
☒	☐	A description of any assumptions or corrections, such as an adjustment for multiple comparisons
☒	☐	The test results (e.g. P values) given as exact values whenever possible and with confidence intervals noted
☒	☐	A clear description of statistics including central tendency (e.g. median, mean) and variation (e.g. standard deviation, interquartile range)
☐	☒	Clearly defined error bars

   See the web collection on statistics for biologists for further resources and guidance.

▶ Software

Policy information about availability of computer code

7. Software

Describe the software used to analyze the data in this study.

> MATLAB r2017a, Mathworks Inc., custom modified diffusion code

For manuscripts utilizing custom algorithms or software that are central to the paper but not yet described in the published literature, software must be made available to editors and reviewers upon request. We strongly encourage code deposition in a community repository (e.g. GitHub). *Nature Methods* guidance for providing algorithms and software for publication provides further information on this topic.

▶ Materials and reagents

Policy information about availability of materials

8. Materials availability

Indicate whether there are restrictions on availability of unique materials or if these materials are only available for distribution by a for-profit company.

> Artemia Salina were obtained from a for-profit company, Mariculture Technologies International.

9. Antibodies

Describe the antibodies used and how they were validated for use in the system under study (i.e. assay and species).

> No antibodies were used.

10. Eukaryotic cell lines

a. State the source of each eukaryotic cell line used.

> No eukaryotic cell lines were used.

b. Describe the method of cell line authentication used.

> No eukaryotic cell lines were used.

c. Report whether the cell lines were tested for mycoplasma contamination.

> No eukaryotic cell lines were used.

d. If any of the cell lines used are listed in the database of commonly misidentified cell lines maintained by ICLAC, provide a scientific rationale for their use.

> No eukaryotic cell lines were used.

▶ Animals and human research participants

Policy information about studies involving animals; when reporting animal research, follow the ARRIVE guidelines

11. Description of research animals

Provide details on animals and/or animal-derived materials used in the study.

> Artemia Salina, male and female, adult-size (1-2 weeks old)

Policy information about studies involving human research participants

12. Description of human research participants

Describe the covariate-relevant population characteristics of the human research participants.

> Study did not involved human research participants.